The Effect of a Glu370Asp Mutation in Glutaryl-CoA Dehydrogenase on Proton Transfer to the Dienolate Intermediate[†,‡]

K. Sudhindra Rao,[§] Zhuji Fu,[∥] Mark Albro,[§] Beena Narayanan,[∥] Saritha Baddam,[§] Hyun-Joo K. Lee,[∥,⊥] Jung-Ja P. Kim,[∥] and Frank E. Frerman*[,§,#]

Departments of Pediatrics and Pharmaceutical Sciences, University of Colorado at Denver and Health Sciences Center, Aurora, Colorado 80045, and Department of Biochemistry, Medical College of Wisconsin, Milwaukee, Wisconsin 53226

Received May 18, 2007; Revised Manuscript Received October 9, 2007

ABSTRACT: We have determined steady-state rate constants and net rate constants for the chemical steps in the catalytic pathway catalyzed by the E370D mutant of glutaryl-CoA dehydrogenase and compared them with those of the wild-type dehydrogenase. We sought rationales for changes in these rate constants in the structure of the mutant cocrystallized with the alternate substrate, 4-nitrobutyric acid. Substitution of aspartate for E370, the catalytic base, results in a 24% decrease in the rate constant for proton abstraction at C-2 of 3-thiaglutaryl-CoA as the distance between C-2 of the ligand and the closest carboxyl oxygen at residue 370 increases from 2.9 Å to 3.1 Å. The net rate constant for flavin reduction due to hydride transfer from C-3 of the natural substrate, which includes proton abstraction at C-2, to N5 of the flavin decreases by 81% due to the mutation, although the distance increases only by 0.7 Å. The intensities of charge-transfer bands associated with the enolate of 3-thiaglutaryl-CoA, the reductive half-reaction (reduced flavin with oxidized form of substrate), and the dienolate following decarboxylation are considerably diminished. Structural investigation suggests that the increased distance and the change in angle of the S−C1(═O)−C2 plane of the substrate with the isoalloxazine substantially alter rates of the reductive and oxidative half-reactions. This change in active site geometry also changes the position of protonation of the four carbon dienolate intermediate to produce kinetically favorable product, vinylacetyl-CoA, which is further isomerized to the thermodynamically stable normal product, crotonyl-CoA.

Glutaryl-CoA dehydrogenase (GCD[1]) catalyzes the oxidation of glutaryl-CoA, an intermediate in the oxidation of lysine, hydroxylysine and tryptophan (*1*). Defects in the enzyme cause glutaric acidemia type I, an often fatal neurologic disease (*1*). It is of interest to understand the mechanism of action of GCD and correlate it with the disease. We have identified E370 in GCD as the general base catalyst that initiates catalysis by abstraction of the *pro-R* hydrogen from C-2 of glutaryl-CoA (*2*−*4*). GCD is inactivated by the mechanism-based inhibitor, 2-pentynoyl-CoA, much more rapidly than inhibition of other acyl-CoA dehydrogenases by the same inhibitor and other 2-acetylenic acyl-CoAs, presumably because GCD catalyzes the net transfer of a proton from C-2 of the substrate to C-4 of the four-carbon dienolate, during catalysis (*4*, *5*).

The rate-determining step in the overall reaction pathway of wild-type GCD is the release of the product, crotonyl-CoA (*6*). The elementary chemical steps catalyzed by wild-type GCD, in sequence, are (a) abstraction of the α-proton of the substrate by the catalytic base, E370, (b) hydride transfer from the β-carbon of the substrate to the N5 of the FAD, (c) decarboxylation of the enzyme-bound intermediate, glutaconyl-CoA, by breakage of Cγ-Cδ bond resulting in formation of crotonyl-CoA dienolate anion and CO_2, and (d) protonation at Cγ of the crotonyl-CoA dienolate intermediate resulting in the product, crotonyl-CoA. FAD is the electron acceptor in the oxidation of the substrate. Reoxidation of the dehydrogenase flavin occurs in two $1e^-$ steps by an external electron acceptor to complete the catalytic cycle. The physical steps involved in the catalytic cycle are (a) binding of the substrate and (b) release of the products, crotonyl-CoA and CO_2. The scheme of the chemical steps is shown previously (*5*, *6*).

[†] This work was supported by grants from the National Institutes of Health, NS39339, and the Children's Hospital Research Foundation to F.E.F. and a grant from the National Institutes of Health, GM29076 to J.-J.P.K.

[‡] The X-ray coordinates and structure factors for E370D GCD−4-NBA (PDB code: 2R0M) and wild-type GCD−3-TGCoA (PDB code: 2R0N) have been deposited in the Protein Data Bank, Research Collaboratory for Structural Bioinformatics, Rutgers University, New Brunswick, NJ.

* Address correspondence to this author at Department of Pediatrics, University of Colorado Health Sciences Center at Fitzsimons, 12800 East Nineteenth Avenue, P18-4404B, Mail Stop 8313, P.O. Box 6511, Aurora, CO 80045-0511. Phone: 1-303-724-3809 or 1-303-724-3807. Fax: 1-303-724-3838. E-mail: Frank.Frerman@UCHSC.edu.

[§] Department of Pediatrics, University of Colorado at Denver and Health Sciences Center.

[∥] Department of Biochemistry, Medical College of Wisconsin.

[⊥] Present address: Chungju National University, Chungju, South Korea.

[#] Department of Pharmaceutical Sciences, University of Colorado at Denver and Health Sciences Center.

[1] Abbreviations: GCD, glutaryl-CoA dehydrogenase; $FcPF_6$, ferricenium hexafluorophosphate (also called ferrocenium hexafluorophosphate; CAS 1287-09-8); HPLC, high performance liquid chromatography; EDTA, ethylenediamine tetraacetic acid, $2Na^+$ salt; 4-NBA, 4-nitrobutyric acid; 4-NBCoA, 4-nitrobutyryl-CoA; 3-TGCoA, 3-thiaglutaryl-CoA.

10.1021/bi7009597 CCC: $37.00
Published on Web 11/17/2007

A conservative substitution of E370 in GCD by aspartate reduces the steady-state turnover of GCD by 95% (*2*). We have examined the effects of the substitution of an aspartate residue for E370 in the initial proton abstraction from 3-thiaglutaryl-CoA (3-TGCoA) by GCD, flavin reduction under anaerobic conditions by transient state kinetics and the steady-state decarboxylation of glutaconyl-CoA. These experiments show that the mutation has relatively little effect on the abstraction of the α-proton from the substrate analogue, 3-TGCoA, by the catalytic base; there is, however, 81% decrease from wild-type value in the net rate constant for the reduction of the flavin that includes deprotonation of the substrate and hydride transfer to the flavin. Significantly, the four-carbon product formed by the reaction catalyzed by the mutant is vinylacetyl-CoA (3-butenoyl-CoA) rather than the normal product, crotonyl-CoA (*trans* 2-butenoyl-CoA). Vinylacetyl-CoA is slowly converted to crotonyl-CoA, the normal product, by an isomerization that is catalyzed by the wild-type GCD as well as the E370D mutant.

The structural bases for these unusual properties of the E370D mutant were elucidated in two structures of GCD complexed with 4-nitrobutyric acid (4-NBA) (hydrolysis product of 4-nitrobutyryl-CoA, 4-NBCoA) and the wild-type complexed with 3-TGCoA. Although the catalytic base in the mutant is only one methylene group shorter than that of wild-type GCD, the structural changes in the arrangement among the catalytic carboxylate, bound ligand and the flavin ring between the two structures provide a rationale for the differences in the catalytic properties.

EXPERIMENTAL METHODS

Enzymes and Reagents. Crotonyl-CoA and glutaryl-CoA were purchased from Sigma. Ferricenium hexafluorophosphate ($FcPF_6$), 4-nitrobutyric acid methyl ester and vinylacetic acid (3-butenoic acid) were purchased from Aldrich. Glutaconyl-CoA was synthesized using glutaconate CoA-transferase according to Buckel and co-workers and purified by chromatography on DEAE cellulose (*7*, *8*). 3-Butenoyl-CoA (vinylacetyl-CoA) was synthesized by the mixed anhydride method (*9*) and purified by chromatography on DEAE cellulose. 3-Thiaglutaryl-CoA (3-TGCoA) and 4-nitrobutyryl-CoA (4-NBCoA) were synthesized and purified as described earlier (*2*, *10*). Purity and analysis of synthetic acyl-CoA esters was accomplished by analytical HPLC (*10*). A small amount of 3-hydroxyglutaryl-CoA (<2%) is present in glutaconyl-CoA, which possibly arises from either a contaminating or intrinsic hydratase activity of glutaconate CoA-transferase (*6*). The retention times of the acyl-CoAs, used in this study, in minutes (average ± standard deviation; n = number of data points) are as follows: 3-hydroxyglutaryl-CoA, 14.2 ± 0.1 (n = 16); glutaryl-CoA, 18.7 ± 0.2 (n = 16); glutaconyl-CoA, 16.2 ± 0.3 (n = 20); 3-hydroxybutyryl-CoA, 19.3 ± 0.1 (n = 22); vinylacetyl-CoA, 24.4 ± 0.1 (n = 19); crotonyl-CoA, 24.9 ± 0.1 (n = 16) (*6*).

Wild-type, E370D and E370Q GCDs were overproduced and purified as previously described (*2*). The proteins were quantitated using ϵ_{447nm} = 14.5, 14.3 and 13.2 mM^{-1} cm^{-1} for the wild-type, E370D and E370Q GCDs, respectively. All other reagents were obtained from commercial sources and were the best grade available. The auxiliary enzymes (enoyl-CoA hydratase, 3-hydroxyacyl-CoA dehydrogenase and thiolase from *Acidaminococcus fermentans*) for the Δ^3,Δ^2-enoyl-CoA isomerase assay were the generous gift of Dr. Wolfgang Buckel, Philipps University, Marburg, Germany (*11*). Recombinant rat liver Δ^3,Δ^2-enoyl-CoA isomerase and rat liver mitochondrial crotonase were kindly provided by Dr. Horst Schulz, City College of New York (*12*, *13*).

Rapid Kinetics. Rapid kinetic reaction measurements were made with an Applied Photophysics SX.18MV Stopped Flow Reaction Analyzer equipped with either a single wavelength absorption photomultiplier or a 256 element photodiode array detector, as described earlier (*6*). Enolate formation, following proton abstraction from 3-TGCoA, yields a charge-transfer species with λ_{max} at ~825 nm (*2*). The net rate constant for the abstraction of the α-proton was estimated by monitoring the formation of the charge-transfer species using the substrate analogue, 3-TGCoA at 25 °C in 50 mM potassium phosphate, pH 7.6 with 5% ethylene glycol (v/v) (*6*). In these reactions, the mutant enzyme was present at 90 μM versus 20 μM for the wild-type enzyme, and pseudo-first-order conditions were maintained. The higher enzyme concentration was necessary because the intensity of the charge-transfer species of the mutant ($\Delta\epsilon_{825}$ = 0.121 mM^{-1} cm^{-1}) at 825 nm is very small compared with that of the wild-type enzyme ($\Delta\epsilon_{825}$ = 5.04 mM^{-1} cm^{-1}), although the K_d of the mutant GCD for the analogue and the K_m for glutaryl-CoA are identical to those of wild-type GCD (*2*). The reductive half-reaction of the flavin by substrate was monitored at 446 nm under anaerobic conditions to determine the net first-order rate constant for flavin reduction at 25 °C in 50 mM potassium phosphate, pH 7.6 with 5% ethylene glycol (v/v). The net rate constants for the oxidative half-reactions of the dehydrogenase flavin were determined at 4 °C following the increase in absorbance at 446 or 447 nm of the $2e^-$ reduced (hydroquinone) mutant GCD when rapidly mixed with $FcPF_6$. The $2e^-$ reduced protein was generated by anaerobic reduction of the dehydrogenase with an equivalent of glutaryl-CoA per flavin. The kinetics of reoxidation of the $1e^-$ reduced dehydrogenase was monitored by following the increase in absorbance at 447 nm of the anionic flavin semiquinone of the dehydrogenase that is stabilized by crotonyl-CoA. The flavin semiquinone was generated by photoreduction of the dehydrogenase/crotonyl-CoA complex at a ratio of 1.0:1.1 under anaerobic conditions in the presence of 10 mM EDTA and 0.5 μM 5-deazariboflavin (*2*, *14*).

Analytical Methods. Glutaryl-CoA dehydrogenase activity was assayed as previously described (*2*). The steady-state rate of decarboxylation of glutaconyl-CoA (75 μM) by E370D GCD was determined at 25 °C in 50 mM potassium phosphate buffer, pH 7.6, as previously described, and the reaction mixture was analyzed by HPLC (*6*). In the conversion of glutaconyl-CoA to vinylacetyl-CoA and subsequent isomerization of vinylacetyl-CoA to crotonyl-CoA, substrate and products were quantitated by HPLC at the indicated times and the first-order rate constants were determined for an irreversible sequential reaction model.

Δ^3,Δ^2-enoyl-CoA isomerase activity of wild-type and mutant GCDs in the steady state was monitored spectrophotometrically at 263 nm ($\Delta\epsilon_{263}$ = 6.7 mM^{-1} cm^{-1}) at 25 °C as described (*15*). Alternatively, crotonyl-CoA formation from vinylacetyl-CoA catalyzed by GCDs was monitored

in a coupled assay following the reduction of NAD^+ at 340 nm ($\Delta\epsilon_{340} = 6.22\ mM^{-1}\ cm^{-1}$) in a 0.5 mL reaction mixture containing 50 mM potassium phosphate, pH 7.6, 2 mM dithiothreitol, 2 mM EDTA, 2 mM NAD^+, 0.2 mM free CoA, 60 μM vinylacetyl-CoA and 160 μg of the auxiliary enzymes from *A. fermentans* (*11*).

The binding constant of GCD for vinylacetyl-CoA was estimated by spectrophotometric titration of E370Q with vinylacetyl-CoA in 50 mM potassium phosphate, pH 7.6 at 25 °C. The E370Q mutant was used because the wild-type and E370D enzymes have significant isomerase and hydratase activity. Binding of vinylacetyl-CoA resulted in the typical red shift of the flavin absorption spectrum that is observed when most acyl-CoA ligands bind to the acyl-CoA dehydrogenases. The binding was monitored at 480 nm, a maximum in the difference spectrum of free enzyme and enzyme saturated with the ligand. Isosbestic points were maintained at 445 and 505 nm. The K_d was determined as previously described (*2*).

Crystallization, Data Collection, Processing, and Structure Refinement. Crystals of the complexes of E370D GCD with ligand were obtained by vapor diffusion using the hanging drop method as previously described for wild-type GCD crystals (*3*). Purified GCD (wild-type or E370D) was dialyzed overnight against a buffer solution containing 20 mM HEPES, pH 7.0, and 100 mM NaCl, and concentrated to a final concentration of 18 mg/mL in the dialysis buffer and 0.1% octyl β-D-glucopyranoside. For the crystals of the mutant (E370D), the protein solution contained 0.5 mM of an alternate substrate, 4-NBCoA. The crystals were obtained by mixing 2 μL of the concentrated protein solution and 2 μL of well solution (containing 100 mM MES buffer, pH 6.5, 30% poly(ethyleneglycol) monomethyl ether 5000 and 0.2 M ammonium sulfate) and equilibrated against 500 μL of the well solution at 19 °C. These crystals were extremely radiation-sensitive and could not be flash-frozen. Therefore, each crystal of the mutant protein was mounted in a glass capillary and diffraction data were collected at 4 °C on an R-AXIS II image plate detector system with a Rigaku RU200 rotating anode generator equipped with an Osmic confocal optics system. The diffraction data from three crystals were processed and merged using DENZO/SCALEPACK (*16*).

Crystals of wild-type GCD complexed with 3-TGCoA were obtained by soaking preformed crystals in the mother liquor solution plus 0.5 mM 3-TGCoA for 2 h prior to data collection (*3*). The data for the E370D GCD−3-TGCoA complex were obtained in a similar manner as that of the wild-type complex but at 100 K from one flash-frozen crystal. Both complexed GCD crystal forms were isomorphous to the previously reported wild-type GCD crystals (*3*) having the space group of $P6_422$, with unit cell parameters of $a = b = 116.9$ Å, $c = 128.1$ Å and $\gamma = 120°$. The asymmetric unit contained one subunit of GCD and the calculated solvent content was 54.5%. The data collection statistics for both data sets along with statistics of structural refinement are given in Table 1. Structures of both GCD complexes were solved by the difference Fourier method using the structure of wild-type GCD (PDB code: 1SIQ) as the starting model (*3*). Multiple rounds of reciprocal space refinement were carried out using CNS (*17*) followed by manual fitting with the graphic visualization program Turbo-Frodo (*18*). The water molecules were picked at electron densities greater than 3σ in the Fo-Fc map after several cycles of model building and structure refinement. The final models were completed with a crystallographic R factor of 0.190 and R_{free} of 0.240 for the E370D GCD−4-NBA, and the corresponding values for the 3-TGCoA complex were 0.209 and 0.273, respectively.

Table 1: Data Collection and Refinement Statistics[a]

GCD complex	E370D GCD−4-NBA	wild-type GCD−3-TGCoA
Data Collection		
resolution (highest resolution shell) (Å)	2.70 (2.80−2.70)	2.40 (2.49−2.40)
no. of total reflections	32297	112427
no. of unique reflections	12017	18755
completeness (%)	81.2 (76.7)	92.1 (84.6)
no. of crystals used for data collection	3	1
$I/\sigma(I)$	7.1 (2.5)	12.7 (2.5)
space group	$P6_422$	$P6_422$
cell dimensions a, b, c; γ (Å; deg)	116.9, 116.9, 128.1; 120.0	114.7, 114.7, 126. 8; 120.0
R_{merge}	0.153 (0.337)	0.070 (0.283)
V_m, solvent content	2.8 Å^3/Da, 54.5%	2.87 Å^3/Da, 52.2%
no. of monomers in asymmetric unit	1	1
Refinement		
no. of protein atoms	3010	3011
no. of water molecules	48	130
no. of bound ligand atoms (FAD)	53	53
no. of bound substrate atoms	9	56
B average		
main chain atoms (Å^2)	24.2	33.5
side chain (Å^2)	25.3	34.1
FAD (Å^2)	21.3	31.5
ligand (Å^2)	36.4	45.5[b]
water molecule (Å^2)	24.5	38.0
$R_{crystal}/R_{free}$	0.190/0.240 (0.312/0.346)	0.209/0.273 (0.320/0.352)
rmsd bond length/bond angle (Å/deg)	0.006/1.18	0.006/1.20

[a] Values in parentheses are for the highest resolution shell. [b] Value obtained using 70% occupancy.

Mass Spectrometry. Mass spectra were determined in the University of Colorado Health Sciences Center's Cancer Center using a PE Sciex API-3000 triple quadrupole mass spectrometer, as described earlier (*5*).

RESULTS

Steady-State Kinetics, Proton Abstraction and Reductive Half-Reaction of GCD. Steady-state kinetic constants for various partial reactions of GCD are summarized in Table 2. The k_{cat} (based on $2e^-$ oxidation of the flavoproteins) for the E370D GCD is 0.28 s^{-1}, compared to 5.6 s^{-1} for the wild-type GCD (*6*). The K_m for glutaryl-CoA is 8 μM at pH 7.6 for both wild-type and E370D GCDs (*6*).

The net rate constant for the abstraction of the α-proton by E370D GCD was estimated using the nonoxidizable substrate analogue, 3-TGCoA, following the increase in absorbance at 800 nm (Figure S1A shown in Supporting Information). The use of 3-TGCoA to estimate the rate of proton abstraction by substrate has been previously described (*6*). Since it has not been possible to experimentally determine the proton abstraction rate directly with the natural

Table 2: Kinetic Rate Constants for Steady-state Turnover and Chemical Steps in the Oxidation of Glutaryl-CoA by Wild-Type and E370D GCDs[a]

reaction	wild-type GCD[b] (s^{-1})	E370D GCD (s^{-1})
steady state		
turnover	5.6 ± 0.3	0.28 ± 0.03
decarboxylation	5.5 ± 0.3	2.04 ± 0.11
isomerization[c]	33.8 ± 1.9	6.04 ± 1.37
chemical steps		
proton abstraction[d]	337.2 ± 37.5	257.1 ± 10.5
flavin reduction[d]	47.6 ± 2.9	9.3 ± 1.3
decarboxylation[e]	−	−
oxidation of $FADH_2$[f]		
from $1e^-$-reduced FAD	267 ± 25	8 ± 1
from $2e^-$-reduced FAD		
first electron	34 ± 13	119 ± 23
second electron	235 ± 23	11 ± 3
redox potential (mV)[b]	-132 ± 8	-131 ± 5

[a] Also, redox potentials are included for ease of understanding. [b] The redox potential refers to that of free enzyme without any ligand. Some of the data is reproduced from Dwyer et al. and Rao et al. (*2*, *6*). [c] Isomerase activity is determined by the method of Buckel (*11*). [d] Proton abstraction from C-2 of 3-TGCoA; flavin reduction includes proton abstraction from C-2 and hydride transfer from C-3 of glutaryl-CoA. [e] 28.6 ± 4.7 s^{-1} for decarboxylation of glutaconyl-CoA with E370Q GCD. The rate constants are averages of multiple determinations over different time scales. [f] Performed at 4 °C with ferricenium hexafluorophosphate as the external electron acceptor.

substrate, 3-TGCoA is a useful tool to compare the rates between wild-type and E370D GCDs. The rate constant for formation of the enolate of 3-TGCoA by E370D GCD is 257 s^{-1}, which is 76% that determined with the wild-type GCD. This result shows that the rate of proton abstraction does not contribute significantly to the decrease in the steady-state turnover. Although the analogue is used to estimate the rate constant for deprotonation of glutaryl-CoA, previous studies with the wild-type protein would indicate that this estimate is neither unusually small or large (*6*). Moreover, the analogue provides a valid comparison of the rates of deprotonation catalyzed by the two enzymes.

The pseudo-first-order net rate constant for flavin reduction, which includes the deprotonation of glutaryl-CoA, catalyzed by E370D GCD under anaerobic conditions is 9.3 s^{-1}, an 81% decrease from wild-type value (Figure S1B and Table 2) (*6*). Aspartate at position 370 is not expected to play a direct role in the chemistry of hydride transfer; however, aspartate substitution has a greater effect on the reductive half-reaction of the dehydrogenase flavin than on the abstraction of the α-proton of the glutaryl-CoA analogue. The spectrum of the protein during the reduction of the flavin suggests a possible reason for the effect on the rate constant of the reductive half-reaction. The extent of reduction by substrate is less than that observed with the wild-type protein, suggesting that internal redox poise is different from the wild-type GCD (Figures S1B and S2). This may also account for the finding that the absorption of the charge-transfer complex in the 500 nm region is less than that of the wild-type protein (*2*, *5*). The E370D mutation also leads to a decrease in the intensity of the charge-transfer band formed by the complex between the E370D GCD and 3-TGCoA (*2*). Our earlier experiments showed that the extinction coefficient of the charge-transfer band at ~800 nm is 42-fold less than that of the complex with the wild-type GCD (*2*). While the aspartate residue plays no direct role in hydride transfer other than maintaining the proper spatial constraints in the active site, it may position the substrate and the acyl-CoA ligand to maintain internal redox equilibria (*19*, *20*) and generate the charge-transfer species.

Oxidation of Reduced Glutaryl-CoA Dehydrogenase. With the wild-type GCD, the two $1e^-$ steps have a rate constant value of 235 ± 23 s^{-1} and 34 ± 13 s^{-1}, the slower step being the transfer of the first electron from the $2e^-$ reduced state and the faster step being oxidation of $1e^-$ reduced semiquinone state (*6*). E370D GCD was anaerobically reduced with equimolar substrate and further oxidized by $FcPF_6$ in the stopped flow spectrophotometer at 4 °C. The large rate constants expected for this oxidation necessitated working at a lower temperature for detection of spectral species. In the case of E370D GCD, the rate constants for oxidation of the $2e^-$ reduced state are 119 ± 23 and 11 ± 3 s^{-1}, while the rate constant for oxidation of the $1e^-$ photochemically reduced mutant GCD in complex with crotonyl-CoA is 8 ± 1 s^{-1} (Figure S3 and Table 2). Thus, it may be inferred that the faster step is the transfer of the first electron from the $2e^-$ reduced E370D GCD. The relative rates of oxidation of the two redox states in the wild-type and mutant GCDs are reversed. The reason for this behavior is not clear. Saenger and co-workers have established that the binding of thioesters regulates the reoxidation of acyl-CoA dehydrogenases (*21*). Thus, the binding of the acyl-CoA ligands again appears different with E370D GCD when compared to wild-type GCD. Again, a change in structure of a binary complex is implicated.

Structure of E370D GCD−Substrate Analogue Complex. The decreased rates of proton abstraction and flavin reduction, the alteration in the mechanism of dehydrogenase flavin oxidation and the decreased intensity of the charge-transfer species suggested that the structure of the ligand−isoalloxazine interaction was altered by the E370D mutation. Charge-transfer complexes between acyl-CoA ligands and the isoalloxazine ring may influence both the oxidative and reductive half-reactions of the acyl-CoA dehydrogenases (reviewed in (*22*)). Therefore, we determined the structure of the complex between the mutant protein and 4-NBCoA and compared this structure with those of the same complex of the wild-type GCD and the complex of wild-type GCD with 3-TGCoA.

The final Fo-Fc omit map showed extra electron densities in the active site at the *re*-side of the flavin, indicating that an acyl ligand was bound to the mutant enzyme (Figure 1A). However, the densities were not sufficient to be fitted for an entire 4-NBCoA molecule, the alternate substrate included in the crystallization medium. While the acyl moiety of the ligand was well defined, the density corresponding to the pantotheine-ribose-adenosine portion of the molecule was not visible. Therefore, 4-NBA, the hydrolysis product of 4-NBCoA, was modeled. Although the crystallization medium contained the alternate substrate, 4-NBCoA, at the relatively high pH of the solution (pH 6.5) and the relatively long duration of the crystallization process, it is not surprising to find the hydrolysis product in the enzyme's active site. Apparently, the alternate substrate/product was bound to the mutant enzyme and hydrolyzed slowly to 4-NBA, which was retained due to its tight binding to the active site cavity through the three hydrogen bonds; two by the carboxylate group and one by the 4-nitro group, in addition to the van

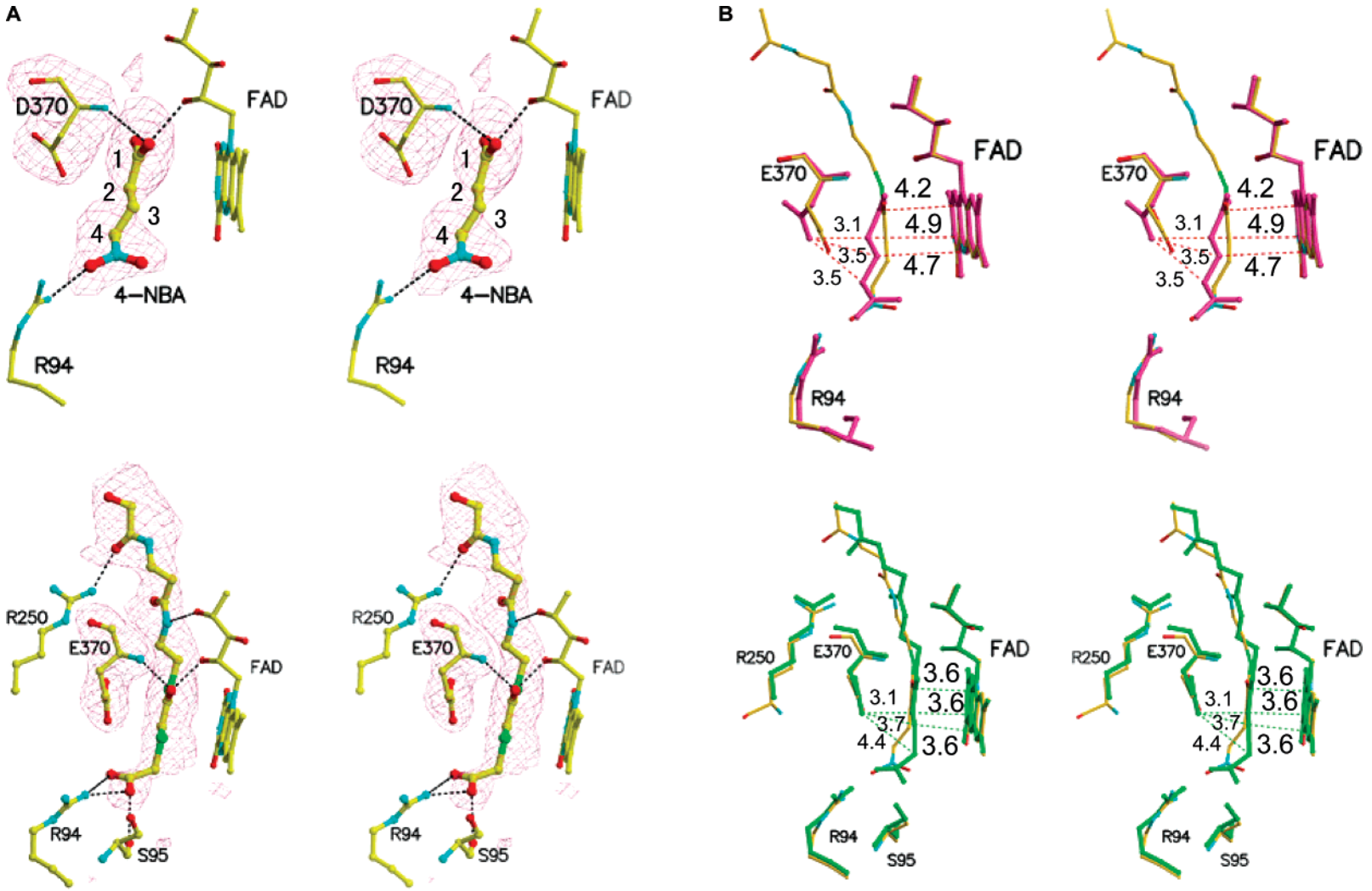

FIGURE 1: (A) Stereodiagrams of the final omit (Fo-Fc) map. Upper panel: E370D GCD complexed with 4-NBA. Lower panel: Wild-type GCD complexed with 4-NBCoA. The electron densities are contoured at 2.5σ. Carbon atoms of the bound ligand are numbered. Hydrogen bonds are shown with black dotted lines. For clarity, only the acyl-pantetheine half of the acyl-CoA ligand is shown. (B) Comparisons of the active sites with that of previously published structure of wild-type in complex with 4-NBCoA (PDB code: 1SIR) (*3*). The structures were aligned by superimposing only FAD. Upper panel: Comparison of E370D GCD−4-NBA with wild-type GCD−4-NBCoA. Lower panel: Wild-type−3-TGCoA and wild-type−4-NBCoA. The distances are marked with dotted lines between C-2, C-3, and C-4 atoms of the ligand to C4a of flavin, carboxylate oxygen and N5 of flavin, and carboxylate oxygen of the catalytic base, respectively. For clarity, the corresponding distances in the wild-typeGCD−4-NBCoA complex structure are not marked. Upper panel: Even considering the overall coordinate errors of ∼0.3 Å for both the mutant and wild-type complexes, as estimated from the Luzzati plots, the distances between C-3 of the ligand and N5 of FAD (4.7 Å) and between C-2 of the ligand and C4a of FAD (4.9 Å) in the mutant are significantly different from those (4.0 Å and 3.9 Å, respectively) in the wild-type−4-NBCoA. The other distances (dotted lines) are similar in the two structures (differences <0.4 Å). The plane of C1(═O)−C2−C3 is parallel to the FAD isoalloxazine ring in the wild-type−4-NBCoA structure (atom color), while that in the mutant structure (pink) is ∼30°. Lower panel: The corresponding distances in the 3-TGCoA complex structure are all very similar to those of the wild-type structure, except for the position of the C-4 atom. The distance between C-4 and the carboxylate oxygen in the 3-TGCoA structure is 4.4 Å, and that in the 4-NBCoA is 3.1 Å. Thus, in the 3-TGCoA complex structure, atoms of C1(═O)−C2−C3−C4 (green) make a perfect plane, which is parallel to the isoalloxazine ring, whereas in the 4-NBCoA complex structure, the C-4 atom is not in the same plane.

der Waals interactions involving the acyl chain (Figure 1A; upper panel). Therefore, the binding mode of 4-NBA to the enzyme active site is comparable to that of the acyl moiety of the substrate/product.

It is not uncommon to find the hydrolysis product of an acyl-CoA substrate/product in the crystal structure of enzyme−substrate/product complex. For example when crystals of the complex of an acyl-CoA oxidase with dodecanoyl-CoA were obtained by cocrystallization methods, dodecanoate, instead of dodecanoyl-CoA, was found in the active site (*23*).

On the other hand, the structure of wild-type crystals soaked in the solution containing 3-TGCoA showed clear density of the entire ligand molecule in the active site cavity. The short time of soaking the crystals and the fact that the active site of the wild-type is more compact presumably prevented hydrolysis of the bound ligand. As expected, the overall polypeptide folds of both structures are the same as those of wild-type GCD with and without bound 4-NBCoA, which we previously determined (*3*). The rms deviations among various GCD complex structures range from 0.19 Å (wild-type GCD−4-NBCoA and E370D GCD−4-NBA) to 0.38 Å (E370D GCD−4-NBA and wild-type GCD−3-TGCoA) for the entire 390 visible Cα atoms. However, the locations of the bound ligand in the active site of the GCD proteins are slightly but significantly different between the wild-type and mutant structures. Figure 1B shows pairwise overlays of the active sites of the three structures, E370D GCD−4-NBA, wild-type GCD−4-NBCoA, and wild-type GCD−3-TGCoA. The structure of wild-type GCD−4-NBCoA in Figure 1B is taken from our previous work and is presented for comparison (PDB code: 1SIR) (*3*). In all structures, the carbonyl oxygen of the thioester ligand or one of the carboxylate oxygens of 4-NBA in the mutant structure forms hydrogen bonds to both the 2′-OH of FAD and the amide nitrogen of the catalytic base, E370 for wild-type or D370 for the mutant, and the 4-nitro group makes a hydrogen bond with R94, indicating that both ligands (4-NBA and 4-NBCoA) are bound to the active site in the proper position and orientation for catalysis. The distances between the γ carbonyl oxygen atom of E370 or β of D370 and C-2, C-3, and C-4 of the acyl-CoA ligand are similar or slightly shorter in the mutant structure (distances in wild-type/mutant, 2.9/3.1 Å for C-2, 3.3/3.5 Å for C-3, and 3.1/3.4 Å for C-4; estimated error 0.3 Å). However, the distances from C-2 and C-3 of the ligand to C4a and N5 of the flavin are 4.9 Å and 4.7 Å in the mutant in comparison to 3.9 Å and 4.0 Å, respectively, in the wild-type GCD. Thus, these distances are much larger in the mutant, indicating that the ligand is pulled toward the catalytic residue by almost 1 Å in the mutant to maintain a similar distance as in the wild-type structure, but is further away from the isoalloxazine ring. It is likely that the increased distance between C-3 of the ligand to N5 of the isoalloxazine ring in the mutant is responsible for the decreased rate constant of flavin reduction (Figure S1B and Table 2; see above).

In computational studies with medium-chain acyl-CoA dehydrogenase, a charge-transfer complex has been shown to involve orbital overlap of the C2−C1−C1═O enolate with the C10a−C4a atoms of the flavin (*24*, *25*). Those distances are increased with the E370D mutant in comparison to the wild-type GCD. Moreover, the planes of the C2−C1−C1═O enolate and isoalloxazine system are parallel in both wild-type structures whereas the two planes in the mutant structure make an approximately 30° angle (Figure 1B). Both the increased distance and angle between the two planes will influence the intensity of the charge-transfer bands and kinetic rate constants.

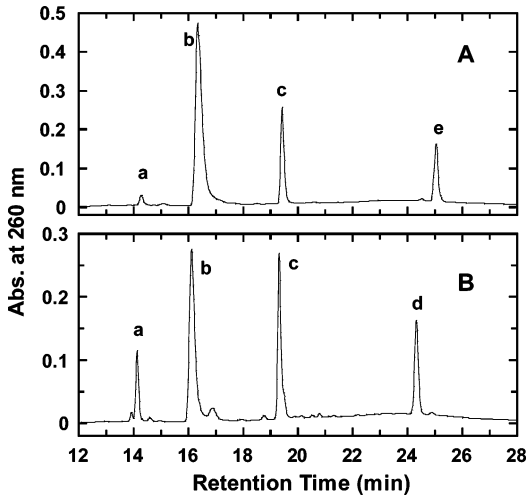

FIGURE 2: HPLC profile of products of decarboxylation of glutaconyl-CoA (75 μM) by (A) wild-type GCD (15 nM) at a reaction time of 135 s and (B) E370D GCD (200 nM) at a reaction time of 479 s. The peaks are (a) 3-hydroxyglutaryl-CoA, (b) glutaconyl-CoA, (c) 3-hydroxybutyryl-CoA, (d) vinylacetyl-CoA, and (e) crotonyl-CoA. The experiments were performed at 25 °C in 50 mM phosphate buffer, pH 7.60. Note that a very small amount of vinylacetyl-CoA and crotonyl-CoA may be seen in the decarboxylation reaction catalyzed by wild-type and E370D GCDs, respectively.

Decarboxylation of Glutaconyl-CoA. Wild-type GCD catalyzes the decarboxylation of glutaconyl-CoA with an apparent k_{cat} of 5.5 s^{-1} expressed as a turnover number (*6*). The single acyl-CoA product of decarboxylation of glutaconyl-CoA by wild-type GCD has been identified as crotonyl-CoA by HPLC (Figure 2A), and crotonyl-CoA was the sole product observed in the single turnover experiments (*5*). Similar experiments were carried out to determine the steady-state rate of decarboxylation of glutaconyl-CoA by E370D GCD. In the initial phase of the decarboxylation reaction, monitored by HPLC, the major product consistently eluted ~32 s earlier than crotonyl-CoA (retention time of the unknown = 24.4 ± 0.1 min in comparison to that of crotonyl-CoA = 24.9 ± 0.1 min) (Figure 2B). The product of decarboxylation of glutaconyl-CoA by E370D GCD, when analyzed by mass spectrometry, had the same molecular mass as crotonyl-CoA (CH_3−CH═CH−C(═O)−SCoA; $C_{25}H_{40}N_7O_{17}P_3S$; exact mass 835.2; $[M - H^+]^-$; $m/z = 834$; $[M + K^+ - 2H^+]^-$, $m/z = 872$) suggesting that it was an isomer of crotonyl-CoA; either the *cis* isomer of crotonyl-CoA, or vinylacetyl-CoA (3-butenoyl-CoA; CH_2═CH−CH−C(═O)−SCoA; $C_{25}H_{40}N_7O_{17}P_3S$; exact mass 835.2), the positional isomer of crotonyl-CoA (data not shown). The unidentified product cochromatographed on HPLC with synthetic vinylacetyl-CoA (data not shown). Further, incubation of glutaconyl-CoA with E370D GCD for a longer period shows formation of crotonyl-CoA with stoichiometric depletion of vinylacetyl-CoA.

Evidence that vinylacetyl-CoA is the primary product of decarboxylation of glutaconyl-CoA in the reaction catalyzed by E370D GCD is shown in Figure 3. At 20 nM E370D

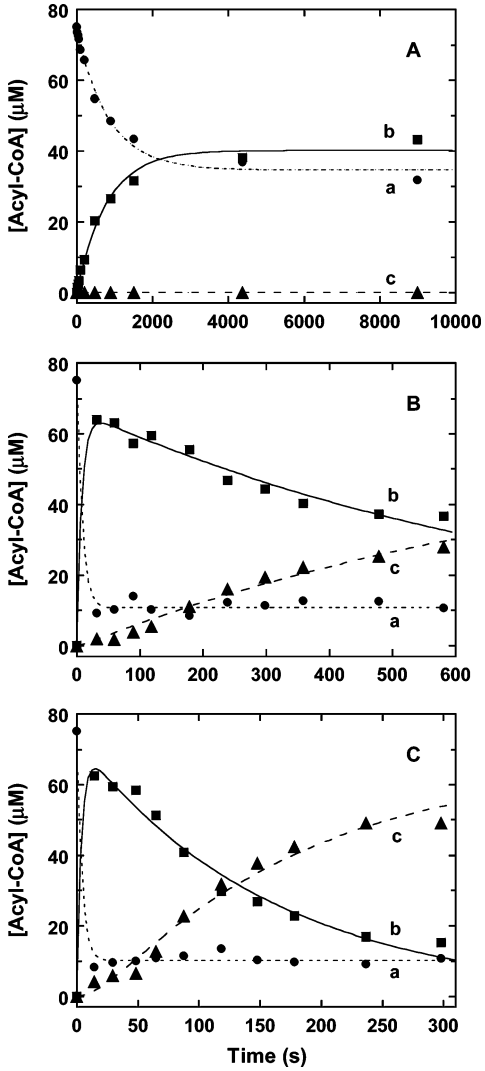

FIGURE 3: Kinetics of decarboxylation of glutaconyl-CoA (75 μM) followed by isomerization of vinylacetyl-CoA to crotonyl-CoA catalyzed by varying concentrations of E370D GCD: (A) 20 nM, (B) 200 nM, and (C) 400 nM. The concentration of the compounds (a = glutaconyl-CoA, b = vinylacetyl-CoA and c = crotonyl-CoA) as a function of reaction time was determined by HPLC (see Figure 2) and the data normalized to a total acyl-CoA concentration of 75 μM. The data were fitted to consecutive irreversible first-order reactions (*26*). Note that only vinylacetyl-CoA is formed with 20 nM E370D GCD and no crotonyl-CoA is present. The experiments were performed at 25 °C in 50 mM phosphate buffer, pH 7.6.

GCD, vinylacetyl-CoA is the sole product of glutaconyl-CoA decarboxylation (Figure 3A). At higher enzyme concentrations (200 and 400 nM), both vinylacetyl-CoA and crotonyl-CoA are detected (Figure 3B,C). At 20 nM E370D GCD, glutaconyl-CoA (75 μM) is decarboxylated to produce exclusively vinylacetyl-CoA, and the initial velocity yields an apparent turnover number (assuming saturation of catalytic concentration of enzyme) of 2.04 s^{-1}. In contrast, the overall steady-state turnover, measured by ferricenium reduction, for the oxidative decarboxylation of glutaryl-CoA by E370D GCD is 0.28 s^{-1} (Table 2) (see below).

The data in Figure 3 was analyzed according to a model for two sequential, irreversible reactions to evaluate the two first-order rate constants, k_1 and k_2:

$$A \xrightarrow{k_1} B \xrightarrow{k_2} C$$

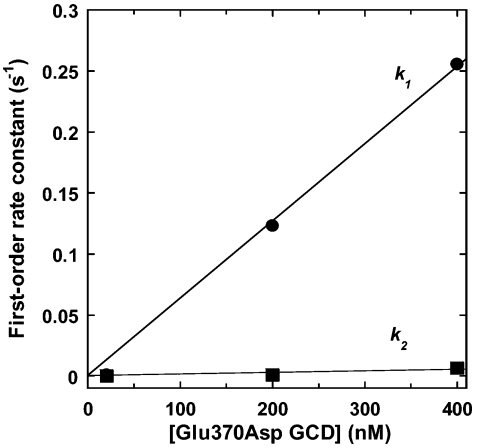

FIGURE 4: Linear fitting of the first-order rate constants, k_1 and k_2, as a function of E370D GCD concentration. The rate constants were obtained from the data in Figure 3. k_1 is the rate constant for decarboxylation of glutaconyl-CoA, and k_2 is the rate constant for isomerization of vinylacetyl-CoA.

where A, B, and C represent glutaconyl-CoA, vinylacetyl-CoA, and crotonyl-CoA, respectively, and k_1 and k_2 are the first-order rate constants for decarboxylation of glutaconyl-CoA and isomerization of vinylacetyl-CoA, respectively, by E370D GCD (*26*). Figure 3 shows the curve fit used to evaluate the two first-order rate constants, k_1 and k_2, as a function of concentration of E370D GCD (20, 200 and 400 nM). The profiles suggest that glutaconyl-CoA is decarboxylated to produce vinylacetyl-CoA, which is then isomerized to crotonyl-CoA. The rate constants, k_1 and k_2, are plotted as a function of E370D GCD concentration (Figure 4). The linear response suggests that (a) decarboxylation and isomerization are catalyzed by the enzyme and (b) the decarboxylation is ~46 times faster than the isomerization.

The free energy of decarboxylation of glutaconyl-CoA, ΔG°_{decar}, is ≈ -7 kcal/mol (*11*), and the free energy of isomerization of vinylacetyl-CoA to crotonyl-CoA, ΔG°_{iso}, is estimated to be $\approx -2.0 \pm 0.2$ kcal/mol, based on isomerization of 1-butene to *trans*-2-butene (*27*). Decarboxylation of glutaconyl-CoA is irreversible. The irreversible nature of isomerization of vinylacetyl-CoA is consistent with the observation that E370D GCD does not catalyze detectable deuterium exchange at the C-4 methyl hydrogens of crotonyl-CoA in D_2O-buffer (data not shown) (see (*5*) for experimental details). The lack of deuterium exchange at C-4 of crotonyl-CoA with E370D GCD indicates that the intermediate dienolate anion cannot be formed in the reverse reaction. Thus, isomerization of vinylacetyl-CoA to crotonyl-CoA is under thermodynamic control because the new double bond is conjugated with the C-1 carbonyl (*28*). The irreversible nature of decarboxylation and isomerization reactions enables analysis of our data according to the two sequential, irreversible first-order reaction model.

The steady-state turnover rate of the oxidative decarboxylation of glutaryl-CoA by E370D GCD is 0.28 s^{-1} while the steady-state turnover number for decarboxylation of glutaconyl-CoA by the mutant is 2.04 s^{-1} (Table 2). In the case of wild-type GCD, the steady-state turnovers of the two reactions are in close agreement (5.5 and 5.6 s^{-1}), indicating that the release of crotonyl-CoA is the predominant rate-determining step (Table 2) (*6*). This raises the question of the identity of the product of the oxidative decarboxylation

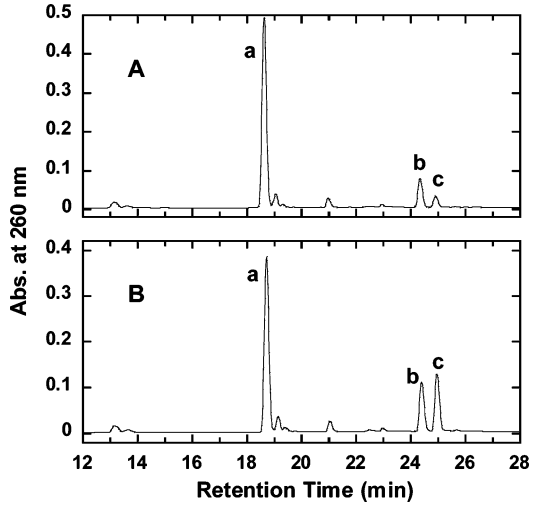

FIGURE 5: HPLC profile of products of turnover of glutaryl-CoA (75 μM) by E370D GCD (400 nM) at a reaction time of (A) 135 s and (B) 479 s. The peaks are (a) glutaryl-CoA, (b) vinylacetyl-CoA, and (c) crotonyl-CoA.

of glutaryl-CoA catalyzed by E370D GCD in presence of $FcPF_6$.

Figure 5 shows the product analysis by HPLC at specific reaction times in the complete turnover of E370D GCD with glutaryl-CoA using $FcPF_6$ as the electron acceptor. With E370D GCD, vinylacetyl-CoA is produced first in the oxidative decarboxylation of glutaryl-CoA; it is then isomerized to crotonyl-CoA (Figure 5). With wild-type GCD only crotonyl-CoA is produced upon oxidative decarboxylation of glutaryl-CoA (*5*, *6*). Thus, mutating the E370 residue to aspartate changes the product profile of the reaction catalyzed by the mutant.

These results may indicate that either (a) the mutation has led to an enzyme that has an intrinsic isomerase activity or (b) the wild-type enzyme may also have isomerase activity. Figure 6 shows the formation of crotonyl-CoA from vinylacetyl-CoA when incubated with either recombinant rat liver Δ^3,Δ^2-enoyl-CoA isomerase (dotted line) or E370D GCD (solid line). The increase in absorbance at 263 nm indicates the formation of α,β-unsaturated acyl-CoA, crotonyl-CoA. Further, addition of rat liver mitochondrial crotonase then indicates a decrease in absorbance at 263 nm due to conversion of crotonyl-CoA, but not vinylacetyl-CoA, to (L)-3-hydroxybutyryl-CoA when α,β-unsaturation is lost due to hydration. The change in absorbance at 263 nm has been quantitated by using $\Delta\epsilon_{263} = 6700\ M^{-1}\ cm^{-1}$ (Figure 6). In this experiment, aliquots were drawn at specific intervals, where no further change in absorbance at 263 nm was seen, and the products quantified by HPLC (Table 3). Table 3 correlates well with the identity and amount of all three acyl-CoAs shown in Figure 6.

The steady-state turnover of Δ^3,Δ^2-enoyl-CoA isomerase activity of wild-type (0.2 nM) and E370D GCD (2.5 nM) was determined using the β-oxidation complex auxiliary enzymes with 60 μM vinylacetyl-CoA. These values were 33.8 ± 1.9 and $6.0 \pm 1.4\ s^{-1}$ for the wild-type and E370D GCDs, respectively (Table 2). That these rate constants were measured under saturating conditions is supported by determination of the dissociation constant of binding of vinylacetyl-CoA to E370Q GCD to be 4.7 ± 0.6 μM as measured

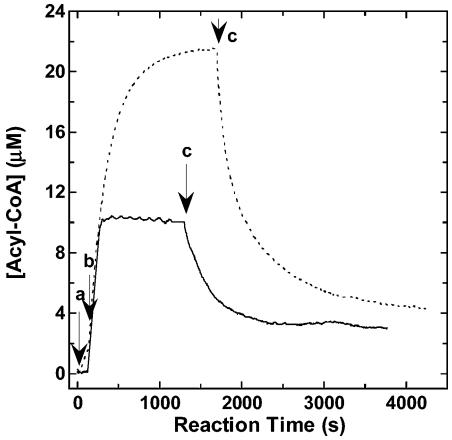

FIGURE 6: Isomerization of vinylacetyl-CoA to crotonyl-CoA catalyzed by E370D GCD (solid line). Absorbance at 263 nm is monitored as a function of reaction time at 25 °C. For comparison, the experiment is also performed with rat liver Δ^3,Δ^2-enoyl-CoA isomerase (dotted line). The reaction mixture (1.2 mL) contained 32 μM vinylacetyl-CoA in 50 mM potassium phosphate buffer, pH 7.6. The arrows indicate the addition of the following enzymes (final amount/concentration) upon the absorbance reaching a plateau: (a) 3.7 mU of rat liver Δ^3,Δ^2-enoyl-CoA isomerase (dotted line), (b) 400 nM E370D GCD (solid line), and (c) 6 U of rat liver mitochondrial crotonase. The change in absorbance at 263 nm is quantitatively converted to concentration of either formation or depletion of 2-enoyl-CoA using $\Delta\epsilon_{263\ nm} = 6.7\ mM^{-1}\ cm^{-1}$. Aliquots (160 μL) were drawn at time points indicated by arrows and quenched with 80 μL of 95 mM phosphoric acid. These samples were further analyzed by HPLC (see Table 3 for results).

Table 3: Product Composition upon Treatment of Vinylacetyl-CoA with Either Authentic Isomerase or E370D GCD and Authentic Crotonase[a]

reaction condition	% VACoA	% CrCoA	% 3-HOBCoA
zero time[b]	82.1	8.4	9.5
+ authentic isomerase	8.7	85.5	5.8
+ authentic crotonase	7.7	17.4	74.9
zero time[b]	88.1	5.4	6.5
+ E370D GCD	63.6	32.0	4.4
+ authentic crotonase	66.2	7.0	26.8

[a] See Figure 6 for details. [b] The synthetic vinylacetyl-CoA (VACoA) is about 85% pure and contains about 5−10% of crotonyl-CoA (CrCoA) and 5−10% of 3-hydroxybutyryl-CoA (3-HOBCoA).

by spectrophotometric titration. Thus, the wild-type GCD does have isomerase activity.

DISCUSSION

Our results show that mutation of the catalytic base of GCD by substitution of aspartate for glutamate 370 (E370D) alters both the net rate constants for chemical steps in the reaction catalyzed by GCD and the product profile of the reaction. Rate constants for the reductive and oxidative half-reactions of the dehydrogenase flavin are decreased. Alteration of product identity can be rationalized by changes in the active site geometry of the catalytic base with respect to the dienolate intermediate (Scheme 1). This results in protonation of dienolate at C-2 rather than C-4 with E370D GCD.

Kinetic and Structural Properties of E370D GCD. The present experiments showed that the net rate constant for flavin reduction is about 5-fold slower than that of the wild-type enzyme (Table 2). This rate constant determined by

Scheme 1: Covalent Bond-Breaking and Bond-Forming Reactions That Occur within the Active Site of E370D Glutaryl-CoA Dehydrogenase during (A) Oxidative Decarboxylation of Glutaryl-CoA That Yields the Kinetically Controlled Product, Vinylacetyl-CoA, and (B) Isomerization of Vinylacetyl-CoA to the Thermodynamically Stable Product, Crotonyl-CoA[a]

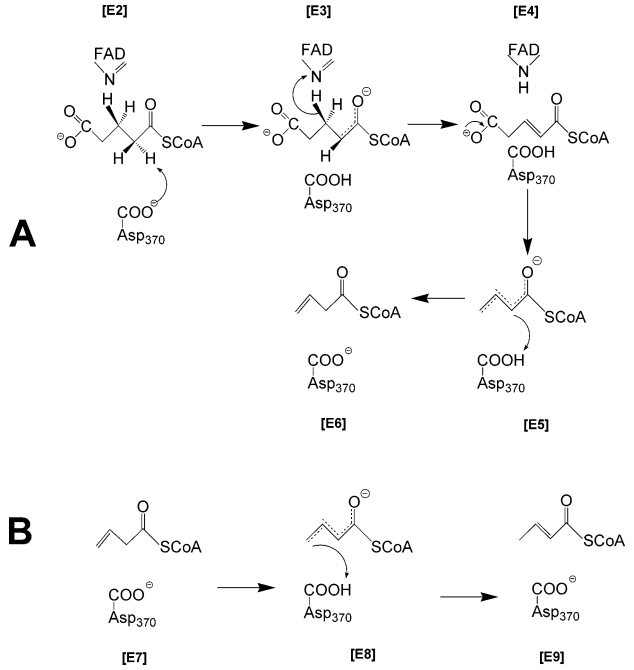

[a] The reoxidation of reduced GCD flavin, which occurs by the external electron acceptor, is not shown. E2−E9 each represents an enzyme species with an acyl-CoA intermediate during the progress of reaction. The binding of the substrate and the release of products are not shown. Vinylacetyl-CoA is released from the enzyme active site from E6. E7 represents the enzyme species that rebinds vinylacetyl-CoA after release from E6.

stopped flow spectrophotometry includes both proton abstraction at C-2 and hydride transfer from C-3 of the substrate to N5 of the flavin. The rate of the model reaction for deprotonation of glutaryl-CoA, i.e., the deprotonation of 3-TGCoA at C-2, shows a relatively small (24%) decrease. However, the rate of flavin reduction is decreased by 81%, suggesting that hydride transfer actually dominates the effect on flavin reduction. The magnitude of this change in the net rate constant for flavin reduction was unexpected. The results suggested that the geometry of the acyl-CoA/flavin complexes in E370D GCD is altered. This alteration was initially inferred from the change in the intensity of the charge-transfer band, which could reflect the altered geometry, especially in the case of the binary complex of E370D GCD with 3-TGCoA. Because there is no large change in the microenvironment of the 3-TGCoA, it is very unlikely that this large change in the charge-transfer band involves a change in the pK_a of the C-2 proton. The diminished intensity of the charge-transfer band in the kinetic experiments and static titration with substrate is more complicated and likely reflects the ligand−flavin geometry in the active site and, in the case of an oxidizable substrate, the difference in the internal redox poise of the mutant enzyme. Efimov and McIntire recently showed clear relationships among charge-transfer interactions, redox potentials, and catalytic activity in *p*-cresol methylhydroxylase (*29*). The C4a−C10a bond of the isoalloxazine ring is the proposed site of overlap of HOMO−LUMO for the formation of the charge-transfer species (*30*). The charge-transfer transition becomes prominent at about the van der Waals contact distance, and any increase in this contact distance would lead to decrease of the charge-transfer absorption band intensity. Although it is not yet clear how charge-transfer species may be involved in catalysis by GCD, the results of the structural and kinetic experiments are consistent with their participation.

Shortening the length of the side chain of the carboxylate catalytic base by ~1 Å, as a result of substitution of aspartate for glutamate, decreased the rate of α-proton abstraction by only 24%; however, the net rate of flavin reduction was reduced by 81%. The crystal structure of the E370D GCD with the substrate analogue, 4-NBA, is consistent with the idea that the mutation affects the positioning of glutaryl-CoA for proton transfer from C-2 and subsequent hydride transfer from C-3. The distance between the catalytic residue and C-2 is only slightly increased (0.2 Å), while that between C-3 and N5 of FAD increased significantly (0.7 Å). Perhaps more importantly, the planes of the C2−C1−C1═O enolate and isoalloxazine system are parallel in wild-type structures, while the two planes make an approximate 30° angle in the mutant structure. In addition to the effects on the reductive half-reaction of the flavin, this positioning would also be expected to influence the oxidative half-reaction, which must involve the semiquinone oxidation state of the dehydrogenase flavin because the physiological electron acceptor, electron-transfer flavoprotein, is a one-electron acceptor. Positioning of the ligand with respect to the flavin would be expected to influence the stability of the dehydrogenase semiquinone. Certainly, the reactions of the $2e^-$- and $1e^-$-reduced E370D dehydrogenase are considerably different from the wild-type dehydrogenase (*6*).

Protonation of the Dienolate Product of Decarboxylation of Glutaconyl-CoA and Isomerization of the Vinylacetyl-CoA by E370D GCD. The position of protonation of the dienolate intermediate formed upon decarboxylation of glutaconyl-CoA by E370D GCD initially yields vinylacetyl-CoA, which is slowly isomerized to crotonyl-CoA. The distance from the carboxyl oxygen of Asp370 to C-4 of the dienolate cannot entirely explain this finding. However, the angle between the plane of the isoalloxazine and extended conjugation of the dienolate following decarboxylation appears to influence the site of protonation of the dienolate. Protonation at C-2 by Asp370(H^+) yields vinylacetyl-CoA, whereas protonation at the C-4 position yields crotonyl-CoA (Scheme 1). As a result of the difference in the angle of the transient dienolate and Asp370 β-carboxyl, we propose that C-2 of the dienolate may be more easily protonated than the C-4 since the resolution of the structure in the C-4 region is relatively low. The formation of vinylacetyl-CoA upon decarboxylation of glutaconyl-CoA is kinetically controlled whereas the isomerization of vinylacetyl-CoA to crotonyl-CoA is under thermodynamic control.

ACKNOWLEDGMENT

We thank Dr. David Jones, School of Medicine, University of Colorado at Denver and Health Sciences Center, Aurora, for NMR work. We thank Dr. Joseph Zirrolli, School of Pharmacy, University of Colorado at Denver and Health Sciences Center, Denver, for mass spectral analysis. We

thank Dr. Horst Schulz of the Department of Chemistry, City College of New York, New York, for a gift of recombinant rat liver Δ^3,Δ^2-enoyl-CoA isomerase and rat liver mitochondrial crotonase. We thank Dr. Wolfgang Buckel, Philipps University, Marburg, Germany, for the auxiliary enzymes (enoyl-CoA hydratase, 3-hydroxyacyl-CoA dehydrogenase and thiolase from *Acidaminococcus fermentans*) used in the Δ^3,Δ^2-enoyl-CoA isomerase assay. We thank Dr. David Ballou, Department of Biological Chemistry, University of Michigan, Ann Arbor, for protocatechuate dioxygenase.

SUPPORTING INFORMATION AVAILABLE

Stopped-flow kinetic data for the formation of the charge-transfer band due to proton abstraction and flavin reduction due to proton abstraction and hydride transfer (Figure S1A,B), spectral titration of E370D GCD by substrate under anaerobic conditions (Figure S2), and stopped-flow kinetic data of oxidation of $1e^-$- and $2e^-$-reduced E370D GCD by $FcPF_6$ (Figure S3). This material is available free of charge via the Internet at http://pubs.acs.org.

REFERENCES

1. Goodman, S. I., and Frerman, F. E. (2001) Organic acidemias due to defects in lysine oxidation: 2-Ketoadipic acidemia and glutaric acidemia, in *The Metabolic and Molecular Bases of Inherited Disease* (Scriver, C. R., Beaudet, A. L., Valle, D., Sly, W., Childs, B., Kinzler, K. W., and Vogelstein, B., Eds.) 8th ed., pp 2195−2205, McGraw-Hill, New York.
2. Dwyer, T. M., Rao, K. S., Goodman, S. I., and Frerman, F. E. (2000) Proton abstraction reaction, steady-state kinetics, and oxidation-reduction potential of human glutaryl-CoA dehydrogenase, *Biochemistry 39*, 11488−11499.
3. Fu, Z., Wang, M., Paschke, R., Rao, K. S., Frerman, F. E., and Kim, J. J. (2004) Crystal structures of human glutaryl-CoA dehydrogenase with and without an alternate substrate: structural bases of dehydrogenation and decarboxylation reactions, *Biochemistry 43*, 9674−9684.
4. Rao, K. S., Albro, M., Vockley, J., and Frerman, F. E. (2003) Mechanism-based inactivation of human glutaryl-CoA dehydrogenase by 2-pentynoyl-CoA: Rationale for enhanced reactivity, *J. Biol. Chem. 278*, 26342−26350.
5. Rao, K. S., Albro, M., Zirrolli, J. A., Vander, Velde, D., Jones, D. N., and Frerman, F. E. (2005) Protonation of crotonyl-CoA dienolate by human glutaryl-CoA dehydrogenase occurs by solvent-derived protons, *Biochemistry 44*, 13932−13940.
6. Rao, K. S., Albro, M., Dwyer, T. M., and Frerman, F. E. (2006) Kinetic mechanism of glutaryl-CoA dehydrogenase, *Biochemistry 45*, 15853−15861.
7. Buckel, W., Dorn, U., and Semmler, R. (1981) Glutaconate CoA-transferase from *Acidaminococcus fermentans*, *Eur. J. Biochem. 118*, 315−321.
8. Klees, A. G., and Buckel, W. (1991) Synthesis and properties of (R)-2-hydroxyglutaryl-1-CoA. (R)-2-hydroxyglutaryl-5-CoA, an erroneous product of glutaconate CoA-transferase, *Biol. Chem. Hoppe-Seyler 372*, 319−324.
9. Fong, J. C., and Schulz, H. (1981) Short-chain and long-chain enoyl-CoA hydratases from pig heart muscle, *Methods Enzymol. 71*, 390−398.
10. Rao, K. S., Vander, Velde, D., Dwyer, T. M., Goodman, S. I., and Frerman, F. E. (2002) Alternate substrates of human glutaryl-CoA dehydrogenase: Structure and reactivity of substrates, and identification of a novel 2-enoyl-CoA product, *Biochemistry 41*, 1274−1284.
11. Buckel, W. (1986) Biotin-dependent decarboxylases as bacterial sodium pumps - Purification and reconstitution of glutaconyl-CoA decarboxylase from *Acidaminococcus fermentans*, *Methods Enzymol. 125*, 547−558.
12. Hubbard, P. A., Yu, W., Schulz, H., and Kim, J. J. (2005) Domain swapping in the low-similarity isomerase/hydratase superfamily: the crystal structure of rat mitochondrial Delta3, Delta2-enoyl-CoA isomerase, *Protein Sci. 14*, 1545−1555.
13. Steinman, H. M., and Hill, R. L. (1975) Bovine liver crotonase (enoyl coenzyme A hydratase). EC 4.2.1.17 L-3-hydroxyacyl-CoA hydrolyase, *Methods Enzymol. 35*, 136−151.
14. Massey, V., and Hemmerich, P. (1978) Photoreduction of flavoproteins and other biological compounds catalyzed by deazaflavins, *Biochemistry 17*, 9−16.
15. Stoffel, W., and Grol, M. (1978) Purification and properties of 3-cis-2-trans-enoyl-CoA isomerase (dodecenoyl-CoA delta-isomerase) from rat liver mitochondria, *Hoppe-Seyler's Z. Physiol. Chem. 359*, 1777−1782.
16. Otwinowski, Z., and Minor, W. (1997) Processing of X-ray diffraction data collected in oscillation mode, *Methods Enzymol. 276*, 307−326.
17. Brunger, A. T., Adams, P. D., Clore, G. M., DeLano, W. L., Gros, P., Grosse-Kunstleve, R. W., Jiang, J. S., Kuszewski, J., Nilges, M., Pannu, N. S., Read, R. J., Rice, L. M., Simonson, T., and Warren, G. L. (1998) Crystallography & NMR system: A new software suite for macromolecular structure determination, *Acta Crystallogr. D 54*, 905−921.
18. Roussel, A., Inisan, A. G., Knoop-Mouthuy, A., and Cambillau, C., Eds. (1999) *Turbo-Frodo, Version OpenGL.1*, CNRS/Universitite, Marseille, France.
19. Gustafson, W. G., Feinberg, B. A., and McFarland, J. T. (1986) Energetics of beta-oxidation. Reduction potentials of general fatty acyl-CoA dehydrogenase, electron transfer flavoprotein, and fatty acyl-CoA substrates, *J. Biol. Chem. 261*, 7733−7741.
20. Schmidt, J., Reinsch, J., and McFarland, J. T. (1981) Mechanistic studies on fatty acyl-CoA dehydrogenase, *J. Biol. Chem. 256*, 11667−11670.
21. Saenger, A. K., Nguyen, T. V., Vockley, J., and Stankovich, M. T. (2005) Thermodynamic regulation of human short-chain acyl-CoA dehydrogenase by substrate and product binding, *Biochemistry 44*, 16043−16053.
22. Ghisla, S., and Thorpe, C. (2004) Acyl-CoA dehydrogenases. A mechanistic overview, *Eur. J. Biochem. 271*, 494−508.
23. Tokuoka, K., Nakajima, Y., Hirotsu, K., Miyahara, I., Nishina, Y., Shiga, K., Tamaoki, H., Setoyama, C., Tojo, H., and Miura, R. (2006) Three-dimensional structure of rat-liver acyl-CoA oxidase in complex with a fatty acid: insights into substrate-recognition and reactivity toward molecular oxygen, *J. Biochem. (Tokyo) 139*, 789−795.
24. Satoh, A., Nakajima, Y., Miyahara, I., Hirotsu, K., Tanaka, T., Nishina, Y., Shiga, K., Tamaoki, H., Setoyama, C., and Miura, R. (2003) Structure of the transition state analog of medium-chain acyl-CoA dehydrogenase. Crystallographic and molecular orbital studies on the charge-transfer complex of medium-chain acyl-CoA dehydrogenase with 3-thiaoctanoyl-CoA, *J. Biochem. (Tokyo) 134*, 297−304.
25. Tanaka, T., Tamaoki, H., Nishina, Y., Shiga, K., Ohno, T., and Miura, R. (2006) Theoretical study on charge-transfer interaction between acyl-CoA dehydrogenase and 3-thiaacyl-CoA using density functional method, *J. Biochem. (Tokyo) 139*, 847−855.
26. Frost, A. A., and Pearson, R. G. (1953) *Kinetics and Mechanism*, John Wiley & Sons, Inc., New York.
27. Benson, S. W., and Bose, A. N. (1963) The iodine-catalyzed, positional isomerization of olefins. A new tool for the precise measurement of thermodynamic data, *J. Am. Chem. Soc. 85*, 1385−1387.
28. Smith, M. B., and March, J. (2001) *March's Advanced Organic Chemistry: Reactions, Mechanisms, and Structure*, 5th ed., Wiley-Interscience, New York.
29. Efimov, I., and McIntire, W. S. (2005) Relationship between charge-transfer interactions, redox potentials, and catalysis for different forms of the flavoprotein component of p-cresol methylhydroxylase, *J. Am. Chem. Soc. 127*, 732−741.
30. Dmitrenko, O., Thorpe, C., and Bach, R. D. (2003) Effect of a charge-transfer interaction on the catalytic activity of Acyl-CoA dehydrogenase: A theoretical study of the role of oxidized flavin, *J. Phys. Chem. B 107*, 13229−13236.

BI7009597